INFRASOUND SOURCE LOCATION USING TIME-VARYING ATMOSPHERIC MODELS

Michael O'Brien and Gordon Shields

Science Applications International Corporation

Sponsored by Army Space and Missile Defense Command

Contract No. DASG60-03-C-0009

ABSTRACT

Advancement of global infrasound event location capabilities for nuclear monitoring has been limited until recently because there were few permanent infrasound stations. The recent completion of several International Monitoring System (IMS) infrasound stations, together with advances in atmospheric propagation modeling, motivated the re-examination of the use of modern atmospheric models in infrasound event signal association, location and analysis.

The first objective of this study was to address known deficiencies in the existing infrasound travel time (TT) tables of Brown (2000) and to generate new tables for all current infrasound stations. The existing tables embody a number of approximations that severely limit their location prediction accuracy. They model only one possible infrasonic arrival as a function of distance, whereas it is well known that infrasound may propagate between the same source and receiver by many paths through effective ducts in the thermosphere, stratosphere and troposphere, each producing different transit times. In addition, the TTs were estimated by ray tracing through the HWM/MSISE climatological atmospheric model (Hedin *et al.*, 1996) but only for four seasons of the year; the diurnal and sub-seasonal variations were not captured. We generated a new tabulation of TTs also based on HWM/MSISE. The Tau9.1 one-dimensional (1-D) ray tracer (Garces *et al.*, 1998) was used to compute TTs from monthly samples of HWM/MSISE at four times of the day. Separate arrival phases were modeled for the two principal atmospheric ducts, thermospheric and stratospheric, but all TTs resulting from multiple-skip paths within each were collapsed to a single TT curve. Uncertainties were estimated from the TT variations calculated in the same manner from time-specific Ground-to-Space (G2S) atmospheric models (Drob, 2003) spanning eight months. Tables were constructed for a total of 19 stations, including 12 recently activated IMS stations. In all over 50 million TTs with uncertainties were computed and arranged into 1704 tables.

The second objective of the study was to evaluate the relative merits of different atmospheric models and approaches to representing them (we refer to this combination as a propagation model) for estimating infrasound event locations in global nuclear monitoring and analysis. We compared the seasonal HWM/MSISE based Brown (2000) model, the new monthly HWM/MSISE based model, a similarly computed but event-specific G2S based model, a constant two-celerity model of 245 and 320 m/s, and the best *a posteriori* fit single-celerity model of 282 m/s. A major difficulty in evaluating location accuracy is the paucity of usable ground-truth events, that is, low atmospheric events for which waveform data, station metadata and well constrained space-time location are available. In this study we compiled data for 21 atmospheric events, from chemical explosions, mining explosions, gas pipe explosions, rocket motor tests and rocket launches, against which to evaluate the predictions of the propagation models. Of these only seven were detected at multiple stations (required for computing an actual location), so we also formulated accuracy measures in terms of predicted TTs and back azimuths.

Overall, the new monthly HWM/MSISE based model performed the best against the data set, followed by the two-celerity model, the event-specific G2S model, the best celerity model, and, finally, the seasonal Brown (2000) model. Counter to expectation, the two-celerity model predicted TTs the best of all models, while the most timely event-specific model was fourth in this respect. In contrast, back azimuth prediction was not very different among the models although all the time-varying models did improve locations and back azimuth residuals over the constant celerity models. We attribute the relatively strong performance of the constant celerity models to the fact that the evaluation dataset is far too small to representatively sample the unmodeled variations related to atmospheric change; thus, our initial results are not likely reflective of the overall predictive abilities of these models. In addition, the TT and back azimuth residuals suggest that collapsing the multiple-skip paths into a single TT curve may be a significant source of error; explicitly modeling them may improve the travel times and back azimuths predicted using HWMS/MSISE and G2S. Further studies are underway to more fully explore these sources of variability.

OBJECTIVES

The first objective of this study was to generate new infrasound travel-time tables for all current infrasound stations based on the HWM/MSISE climatological atmospheric model to address known deficiencies in the existing tables. These travel times are used for locating infrasound events.

The second objective of the study was to evaluate the relative merits of travel times based on different atmospheric models for estimating infrasound event locations in global nuclear monitoring and analysis.

RESEARCH ACCOMPLISHED

Locating events using infrasound arrivals is challenging because wave propagation in the atmosphere is highly variable in both space and time; this is mainly the result of variations in wind and temperature that change the local sound velocity field. Propagation paths, times, and amplitudes are all observed to vary strongly with each of geographic position, direction of propagation, time of day, time of year, and current weather conditions. Moreover, for any source-receiver combination there are almost always multiple propagation paths by which energy may reach the receiver. Thus, there are several elements that contribute to errors in predictions of the infrasound observables (travel time and back azimuth) and source locations computed from them: 1) the atmospheric sound velocity model, 2) the way that model is sampled, 3) approximations in representing the observables from multiple propagation paths, and 4) the method of numerical propagation used to convert sound velocity into infrasound observables. We refer to a single specification of the set of these elements as a “propagation model”.

The difficulties are compounded when using infrasound in systematic global signal association and event location because the association of measured signals with hypothesized events is ultimately inferred from consistency with the hypothesized event location and time. As a result, the consistency of virtually all possible event locations and times must be evaluated. In the U.S. National Data Center association software this is done as an exhaustive global search. It is computationally expensive and, practically, requires that knowledge of the propagation medium be rendered in advance into predicted travel times and deviations between observed and source-receiver back azimuths at each receiver location for energy traveling via all possible paths from all possible source locations. The more dynamic the propagation medium, the more frequently it must be sampled and the less manageable the tabulation becomes. For infrasound in particular, there is an unavoidable trade-off among accuracy, timeliness and computational cost and complexity that affects the choice of each element of a propagation model.

In this paper we present a new tabulation of infrasound travel times, intended for use in global association and location, that improves upon the prediction capabilities of the existing Brown (2000) travel times without affecting timeliness of results or unacceptably increasing computational or logistical cost. First we discuss the trade-offs relating to each propagation model element and present the rationale behind our choices for creating the new travel-time tables. We then present a comparison of predictive capabilities of this propagation model to four others of lesser and greater complexity, including that of the Brown (2000) travel times, to assess the achieved and potential improvements associated with adopting more complexity. We did not tabulate back azimuth information but did include predicted corrections in the evaluation.

Propagation of Infrasound and Atmospheric Sound Velocity Models

The most important element of a propagation model is the atmospheric velocity model. The left panel of Figure 1a illustrates typical atmospheric velocity profiles with zones of increasing velocity that create propagation ducts. Typical propagation paths in the right panel illustrate the most prominent thermospheric and stratospheric ducts. The thermospheric duct exists between all source-receiver combinations at all times; the stratospheric duct exists only under the right wind conditions, which depend on time of day, time of year, propagation direction, and current weather. Tropospheric ducts are much less commonly predicted and occasionally are inferred from observations.

Until recently, the best global atmospheric characterization was provided by HWM/MSISE, a combination of the Horizontal Wind Model (HWM-93) (Hedin et al., 1996) and the Extended Mass Spectrometer - Incoherent Scatter Radar (Picone et al., 2002). This model estimates atmospheric state properties globally up to about 200 km altitude for all times of the year, obtained from averaging across many years of atmospheric observations. For infrasound propagation HWM/MSISE can provide an estimate of the vector sound speed anywhere for any time. However, it predicts only long-term averages of sub-annual trends (diurnal to seasonal), so it has inherent inaccuracy with

respect to the velocity field at any specific time. HWM/MSISE was employed by Brown (2000) at which time it was the only velocity model available. More recently the Naval Research Laboratory (NRL) began generating the Ground to Space (G2S) atmospheric models (Drob, 2000) that fuse lower atmospheric numerical weather prediction results for a specific epoch in the lower 50 km of the atmosphere at (Figure 1b, panel A) with the average trends predicted by HWM/MSISE in the upper atmosphere (Figure 1b, panel B) to produce a single time-specific model of the atmosphere (Figure 1b, panel C). In principle, each G2S model provides more accurate stratospheric propagation velocities at its epoch than HWM/MSISE, and should lead to better prediction of the stratospheric duct and of infrasound observables in general. However, G2S is inherently limited with respect to timeliness of availability for the near-real-time data processing and analyses done in a global monitoring system. For this reason we based the propagation model for the new tabulation of global travel times on HWM/MSISE.

Other velocity models were used to assess their relative potential in an infrasound monitoring system. We based one propagation model on the G2S models because they are presumed to be the most accurate. We also based a propagation model on constant celerities (average horizontal propagation speed) of 245 and 320 m/s for thermospheric and stratospheric arrivals, respectively; this is the simplest model that accounts explicitly for two principal propagation ducts. Finally, we based a propagation model on the single celerity (282 m/s) that best fit the evaluation data set to assess how much of the observations require the complexity in other models to be explained.

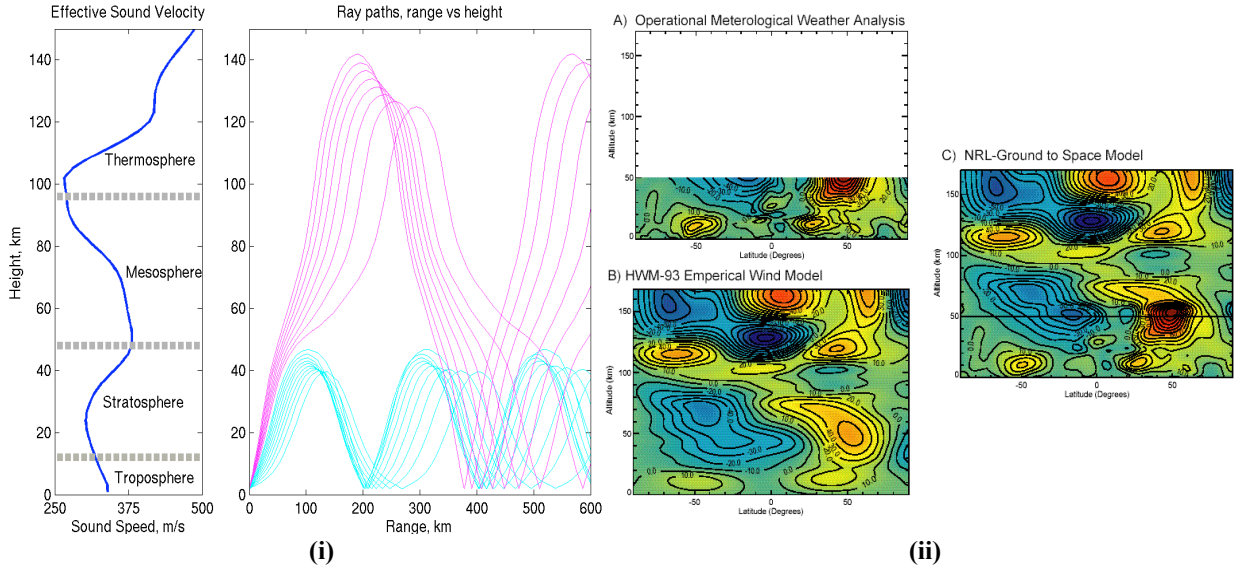

Figure 1. Features and predictions of atmospheric models.

(i) A typical velocity profile in the left pane and predicted ray paths for stratospheric (blue) and thermospheric (purple) arrivals in the right; note the multiple return paths for distance >400 km. (ii) Zonal sound velocities (figure from Drob (2003)) illustrating the construction of G2S models (panel C) from the Operational Weather Analysis data (panel A) and the HWM-93 climatological model (panel B); note the low altitude detail provided by weather data, which can significantly affect stratospheric paths and travel times.

Sampling Atmospheric Models

The innate spatial and temporal limitations of the atmospheric model are compounded by a further sampling performed in its exploitation. Brown (2000) chose to represent travel times at only four times of the year in his seasonal tables, computing travel times from HWM/MSISE sampled once in each season. This misses the important diurnal and sub-seasonal variations altogether, so we chose to sample HWM/MSISE each month at four times of the day (48 averages) to better capture these variations in the new global travel times. This is not an issue for G2S models, which are time specific, or for the constant celerity models, which have no spatial or temporal variations.

Spatial variability is accounted for in a propagation model by predicting travel times and back azimuth deviations at discrete azimuths and ranges from each station. For the global tables, we computed the travel times at azimuths every 1° and ranges every 1.5° from the station out to 120° to accommodate arrivals from large, distant sources. The range discretization was finer for the other propagation models, depending on the event and station.

Approximating Observables from Multiple Propagation Paths

There are almost always multiple paths by which infrasound may propagate from source to receiver with different travel times. This is apparent in Figure 1a at ranges beyond 400 km. The most significant travel-time differences are between stratospheric and thermospheric paths in general. Travel times are typically 10 to 20% smaller for stratospheric paths, due simply to the relative heights and thicknesses of the two ducts. When the stratospheric duct exists, its arrivals are typically stronger than thermospheric arrivals, leading Brown (2000) to a representation of travel times that uses the average stratospheric travel time if predicted for a given azimuth and range, and the average thermospheric travel time otherwise. Thus, where the stratospheric duct is erroneously predicted, travel times for the wrong duct are assigned. We represented times for the two ducts separately in the new HWM/MSISE and G2S propagation models, to allow the more consistent time to be chosen where the duct is predicted.

Skipping within each duct also produces multiple propagation paths with different travel times at a given distance. The effect is illustrated in Figure 2a for thermospheric arrivals. Accounting for each of these separately would multiply the tabulation volume – the spatial and temporal resolution described above for 19 existing stations implies ~25 million travel times per phase which pushes the limitations of existing software, so we opted to represent all the possible travel times within each duct by a single average phase, determined by linear fit to predicted travel times, similar to that shown in the figure. Thus, we represented travel time for each station, time, azimuth and range by two possible phases, "It" for thermospheric paths and "Is" for stratospheric paths where that duct is predicted to exist.

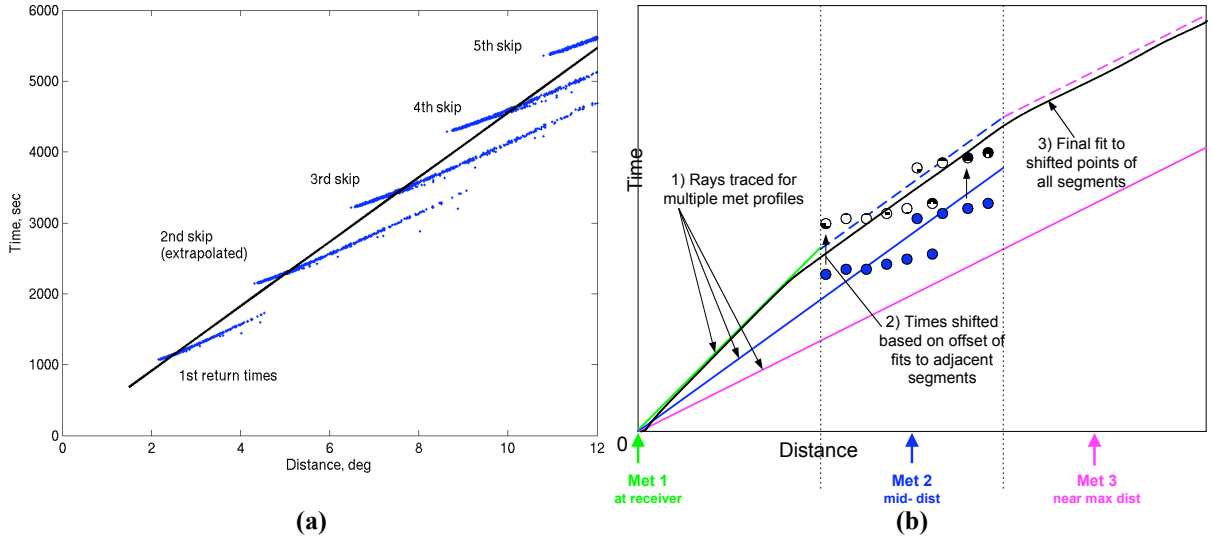

Figure 2. Computation of HWM/MSISE and G2S travel times.

(a) Approximating travel times for multiple skip paths within the thermosphere by a single travel-time curve and (b) accounting for range dependence using Tau9.1 (Garces et al., 1998). The large number of potential skip phases motivated our approximation of a single phase per duct; the large distance range desired in the travel-time tables motivated our approach to accommodate range dependence in the meteorological model.

Methods for Numerical Propagation of Infrasound

There are several methods for numerically propagating infrasound in a non-uniform medium to predict travel times and back azimuths, ranging in complexity from one-dimensional ray tracing to full wave field propagation. Most of these are computationally intensive and were impractical for computing the 50 million travel times of the new global tables – we estimated several months of CPU time to compute them via the HARPA three-dimensional ray tracer of Jones (1986). To make the computation practical we used the Tau9.1 one-dimensional ray tracer, developed at the Infrasound Laboratory at the University of Hawaii (Garces et al., 1998, Hetzer and Garces, 2002), to compute all HWM/MSISE and G2S travel times and back azimuth deviations. Based on the Tau-P method, Tau9.1 solves for the turning points of rays as a function of their takeoff angle assuming a laterally invariant velocity profile; it sums the contributions of each vertical layer to yield time, distance and lateral path offset (azimuth deviation) from translation of the wave front by cross winds. Times for skips through a duct are multiples of the first ground-to-ground traverse. Tau-P does not model time and azimuth effects of wave front bending or accumulated along-path velocity variation.

Along-path velocity invariance is a more serious limitation because it inherently limits the range within which predicted travel times are usefully accurate. To compensate for this we applied Tau9.1 in a crude but computationally cheap approximation of 2-D propagation, as illustrated in Figure 2b. The full 120° distance range was divided into three or four sub-ranges (green, blue and magenta in the figure) and selected a single velocity profile to represent each sub-range. Within each range, travel times were computed (filled circles) using the corresponding velocity profile and a straight line fit to them (dashed lines). The slopes were then spliced together (solid lines) and the resulting curve anchored at zero distance and zero time. The raw travel times were then shifted as were the straight lines (open circles). A fourth order polynomial was fit (not shown) to these over the full distance range and sampled to produce all the HWM/MSIS and G2S travel times. This procedure was performed separately for thermospheric and stratospheric ducts to yield travel-time curves for "It" and "Is" phases respectively. Examples are illustrated in Figure 3. Panel (a) illustrates the typically minor perturbation of our 2-D approach on the constant-slope 1-D results. Figure 3b illustrates typical differences between G2S and HWM/MSISE predicted travel times (G2S predictions are often systematically slower) and back azimuths at which a stratospheric duct is predicted.

To obtain back azimuth deviations, we averaged the first-skip back azimuths predicted for all three profiles. Thus, we estimated only one correction per back azimuth.

Travel-Time Uncertainties

Uncertainties on travel times are necessary for computing confidence limits on source locations. We estimated uncertainties for the global travel times for a given month and time of day as the spread in the travel times predicted by all the available G2S models from the same month and time of day, essentially a superposition of many sets of travel times like that in Figure 2a. In all we used 556 G2S (6-hour) epochs spanning about eight months. For months in which G2S models were not available, we used the spread over the other eight months at the same time of day. The uncertainties thus reflect errors relating to unmodeled temporal variations and to approximations we made in representing multiple skip paths with a single travel time. In contrast, we assumed the skip-path approximations to be the primary source of error in G2S-based travel times and computed the uncertainties for each epoch as the spread among its predicted multiple skip paths, essentially a single set of travel times similar to that in Figure 2a. Note in Figure 3b that the two estimates are almost the same, indicating that more uncertainty relates to averaging the multiple skip times into a single phase, than to unmodeled temporal variations.

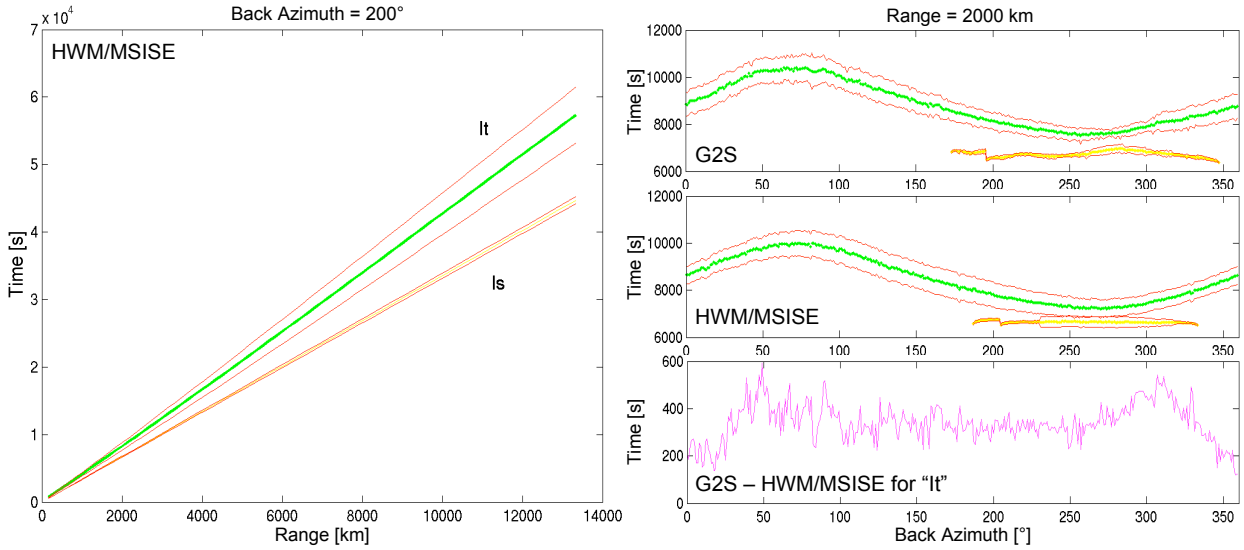

(a) **(b)**

Figure 3. New HWM/MSISE and G2S travel times at station DLIAR, New Mexico.
Travel times predicted for an event on January 23, 2003 20:00 at DLIAR as function of (a) range at back azimuth 200º and (b) back azimuth at range 2000 km. Stratospheric times are yellow, thermospheric times are green, and 1_ confidence limits are red. The stratospheric duct producing "Is" is predicted only within a finite back azimuth range that is roughly downwind. Note the differences between G2S and HWM/MSISE predictions of travel time and range of back azimuths at which stratospheric arrivals are predicted.

Summary of Propagation Models

The five propagation models for which we computed travel times and back azimuth deviations are summarized in Table 1. Global tables were constructed only for the Monthly/TOD (time-of-day) model, although as a consequence of their trivial nature, travel times for the Two-Celerity and Best-Celerity models are time, station and azimuth independent. The event-specific travel times were tabulated only for epochs, ranges, and stations relevant to the data set.

Table 1. Propagation Models Used to Generate Travel Times Sets

Propagation Model	Velocity Model	Sampling			Phases	Propagation Method
		Time	Azimuth	Distance		
Event-Specific	G2S	event times	as needed	as needed	Is, It	Tau9.1 + linear fit
Monthly/TOD	HWM/MSISE	1 per month / 4 per day	1°	1.5°	Is, It	Tau9.1 + linear fit
Seasonal	HWM/MSISE	4 per year	1°	1.5°	I	as in Brown (2000)
Two-celerity	245, 320 m/s	1 for all time	N/A	N/A	Is, It	N/A
Best celerity	282 m/s	1 for all time	N/A	N/A	I	N/A

Evaluation Data Set

We compiled a data set against which to evaluate and compare the predictive capabilities of the propagation models investigated here. The set consists of 21 events, including 32 arrivals, listed in Table 2, for which independent ground truth locations and times are known. The "GT" column indicates uncertainty on the true location. Prior to the evaluation, arrival times and back azimuths were carefully estimated for all 32 detections.

Table 2. Evaluation Data Set

Event	Date	Time	Latitude [°]	Longitude [°]	GT [km]	Detecting Stations
WSMR chemical explosion, New Mexico	11/19/97	18:00:00	33.621	-106.480	1	2
Titan IVB rocket launch, VAFB, California	05/22/99	9:36:00	34.7	-120.6	100	2
Atlas II AS rocket launch, VAFB, California	12/18/99	18:57:00	34.7	-120.6	100	2
Space Shuttle rocket launch, KSC, Florida	10/11/00	23:17:00	28.49	-80.58	100	2
Watusi chemical explosion, NTS, Nevada	09/28/02	21:25:17	37.099	-116.092	1	5
Thiokol plant rocket motor test, Utah	01/23/03	20:00:20	41.626	-112.392	2	3
Chemical explosion, Billy-Berclau, France	03/27/03	5:15:00	50.511	2.881	1	2
Argyle mine explosion, Australia	09/22/96	7:07:29	-16.987	128.357	15	1
WSMR chemical explosion, New Mexico	11/12/97	17:47:00	33.621	-106.450	1	1
Gas pipe explosion, New Mexico	12/12/98	12:55:00	35.4	-108.4	5	1
WSMR chemical explosion, New Mexico	02/25/99	18:20:00	33.679	-106.523	1	1
Hector Mine earthquake, California	10/16/99	9:46:46	34.541	-116.361	100	1
NTS chemical explosion, Nevada	12/08/99	19:29:58	37.012	-116.196	1	1
WSMR chemical explosion, New Mexico	12/09/99	19:00:00	33.681	-106.523	1	1
Gas pipe explosion, New Mexico	08/19/00	11:26:19	32.038	-104.029	1	1
Seattle earthquake, Washington	02/28/01	18:54:34	47.234	-122.521	100	1
Chemical explosion, Toulouse, France	09/21/01	8:17:57	43.62	1.37	20	1
Argyle mine explosion, Australia	04/16/02	9:08:58	-16.751	128.426	10	1
Powder River Basin mine explosion, Wyoming	08/27/02	20:06:53	43.52	-105.27	10	1
Powder River Basin mine explosion, Wyoming	02/12/03	18:59:28	43.75	-105.37	10	1
Powder River Basin mine explosion, Wyoming	03/13/03	19:10:35	43.618	-105.196	10	1

Comparison of Model Predictions

The mean absolute residuals between the predictions of five propagation models in Table 1 and the ground-truth events in Table 2 are listed in Table 3. Locations were computed for the 7 multiply detected events (18 arrivals) using arrival times and observed back azimuths, uncorrected and corrected. The travel-time and back azimuth residuals were averaged over all 32 arrivals. Arrivals were assigned the phase, "It" or "Is", with the best matching travel time for each propagation model that distinguished between them, the Two-Celerity, Monthly/TOD and Event-Specific models. For the Best-Celerity model, arrivals were assigned the Event-Specific phase designations. Travel-time residuals were normalized by the ground-truth travel times to compensate for their distance dependence. Counter to expectation, the Two-Celerity model was the best predictor of locations and travel times, and the most complex Event-Specific model was almost the worst. The expected improvement with model complexity is seen only in back azimuth residuals and locations using corrected back azimuths. However, in any sense, varying the complexity of the propagation model resulted in no more than 20% reduction in the residuals.

Table 3. Mean Absolute Residuals from the Evaluation Data Set

Propagation Model	Location Residuals [km]		Travel-Time Residuals [%]	Back azimuth Residuals [deg]
	Back Azimuth Uncorrected	Back Azimuth Corrected		
Event-Specific (G2S)	170	161	8.9	5.7
Monthly/TOD (HWM/MSISE)	142	139	8.3	5.8
Seasonal (HWM/MSISE)	161	155	9.5	5.7
Two-Celerity (245 / 320 m/s)	129	129	7.7	6.9
Best-Celerity (282 m/s)	178	178	8.1	6.9

Assessment of overall prediction capability is difficult from Table 1 because the four statistics are based on different subsets and kinds of the data. As a result, the significance of the differences between models is unclear. To put all the data on equal footing, to allow all the data to be combined together, and to estimate the significance of differences between model predictions, we constructed the following travel-time and back azimuth statistics:

$$F_t = \frac{\sum_{k=1}^{N}\left(\frac{\Delta t_{ik}}{T_k}\right)^2}{\sum_{k=1}^{N}\left(\frac{\Delta t_{jk}}{T_k}\right)^2} \sim F_{N,N} \qquad F_a = \frac{\sum_{k=1}^{N}\Delta a_{ik}{}^2}{\sum_{k=1}^{N}\Delta a_{jk}{}^2} \sim F_{N,N} \qquad F_{ta} = \frac{\sum_{k=1}^{N}\left\{\left(\frac{\Delta t_{ik}}{T_k}\right)^2 + \Delta a_{ik}{}^2\right\}}{\sum_{k=1}^{N}\left\{\left(\frac{\Delta t_{jk}}{T_k}\right)^2 + \Delta a_{jk}{}^2\right\}} \sim F_{2N,2N}$$

Here, i and j denote any two of the five propagation models, k sums over the N=32 arrivals, Δt_{jk} and Δa_{jk} are the travel-time and back azimuth residuals predicted by the j^{th} model for the k^{th} arrival, and T_k. is the ground-truth travel time for the k^{th} arrival. If the unsquared elements in each denominator and numerator are independently drawn from the same standardized normal distribution then F_t, F_a, and F_{ta} have the indicated F distributions. We can evaluate each statistic, as computed from our limited data sample, against percentage points of F to evaluate the confidence at which one model is indeed a better predictor than another of travel time, back azimuth, or both. To first order we expect Δt_{jk} to linearly increase with distance so that the $\Delta t_{jk}/T_k$ (the fractional along-path errors) should be similarly distributed for a given model j. Also, small Δa_{jk} approximate the fractional cross-path location errors, since, for source-receiver distance d_k, $d_k \sin(a_{jk})/d_k \cong \Delta a_{jk}$. Thus, we expect the Δa_{jk} and $\Delta t_{jk}/T_k$ to be distributed similarly to one another. Table 3 confirms that they have similar size. We assume *a priori* that each population is normally distributed and that the errors in ground truth locations are small compared to those resulting from the propagation model. Confidence limits so obtained will at least have the correct sense and approximately indicate relative ability.

The confidence levels at which one propagation model is a generally better predictor than another of travel times, back azimuths, and both are listed in Table 4. Each cell contains the confidence level at which the row model is a better predictor of the indicated quantity than the column model. Confidence in the converse is given by 100% minus the stated value. The row models are ordered most to least complex and the columns least to most complex, so that for each cell the row model is expected to be a better predictor than the column model, based on that complexity, and, thus to have a value greater than 50%. To highlight results versus expectation, cells are colored green where the expectation is clearly upheld (confidence of 70% or higher), yellow where the result is ambiguous (confidence between 30 and 70%) and red where the expectation is clearly violated (confidence 30% or lower).

Table 4. Confidence Level (%) at which the Row Model is a Better Predictor than the Column Model

Row Model \ Column Model	Best-Celerity 282 m/s	Two-Celerity 245, 320 m/s	Seasonal HWM/MSISE	Monthly/TOD HWM/MSISE
Travel Time				
Event-Specific (G2S)	24	7	42	14
Monthly/TOD (HWM/MSISE)	64	35	81	
Seasonal (HWM/MSISE)	30	10		
Two-Celerity (245, 320 m/s)	77			
Back Azimuth				
Event-Specific (G2S)	70	70	55	56
Monthly/TOD (HWM/MSISE)	65	65	49	
Seasonal (HWM/MSISE)	66	66		
Two-Celerity (245, 320 m/s)	50			
Travel Time + Back Azimuth				
Event-Specific (G2S)	51	38	52	31
Monthly/TOD (HWM/MSISE)	70	58	71	
Seasonal (HWM/MSISE)	49	35		
Two-Celerity (245, 320 m/s)	64			

Table 4 reinforces the indications of Table 3. The new Monthly/TOD propagation is a better overall predictor than the Best-Celerity, Seasonal, and Event-Specific models but at a confidence of only ~70%; it is not much different than the Two-Celerity model. The existing seasonal model of Brown (2000) is the worst. However, most results are not dramatic and some are ambiguous. The most advanced Event-Specific model is consistently the best predictor of back azimuth at confidences up to 70% but is significantly a worse predictor of travel times at confidences as high as 93%. Each time-varying model is better than the static models at estimating back azimuth but only marginally at confidence of 60 to 70%. Some insight into these results can be obtained from examination of the fractional travel-time and azimuth residuals in Figure 4. Residuals are color coded by the phase, “Is” or “It”, assigned to them.

First, it must be noted that the evaluation data set is quite small (32 arrivals) relative to the amount of spatial and temporal variability inherent in infrasound propagation. Thus, the population of arrival data as a whole may not be well represented by this data set and pathological behavior with respect to one or more of the models may be the result. If true, simple, constant celerity propagation models might be expected to perform comparatively well on this data sample but to break down as the sample size increases and becomes more representative of the population. For example, the Event-Specific model predicted travel times very well for a large group of arrivals (the spike of small residuals), but substantially underpredicted another. This could be a fortuitous result of the composition of the data set. However, it may also be result of systematic biases inherent in the propagation models, discussed next.

The most significant approximation we made in computing travel times and back azimuths, was averaging the arrival curves from multiple skip paths into a single curve, as in Figure 2a. It is possible that, in doing so, we have introduced a significant source of error into the thermospheric predictions, by averaging away significant, resolvable detail. This conjecture is supported by features of the travel-time and, to a lesser extent, the back azimuth residuals. First, the inferred “Is” and “It” residuals (blue and red, respectively) have distinctly different distributions for all five models; in each case the “Is” residuals are more compactly and simply distributed. This is consistent with model predictions for significantly more variation among thermospheric than stratospheric travel times and back azimuths of multiple skip paths, as illustrated in Figure 3 – the predicted spread among “It” skip travel times is typically about 10 to 15%, which is about the size of the “It” residuals in Figure 4. In fact, if the “It” residuals are dominated by this source of error, then their uneven distributions are also expected since only a few discrete arrival times are predicted for any source-receiver scenario. The observed biases in the “It” residuals further support this. Since no formal accounting was made for the predicted amplitudes of the skip arrivals, hence their likelihood of being detected, a bias proportional to the spread among the skip travel times is inevitable in fitting as we did. The widely spread “It” yield produce large biases, while the tightly confined “Is” skips yield almost none. This suggests simply replacing the duct-averaged phases we chose to use with skip-specific phases. However, the validity of such a representation hinges on being able to accurately estimate amplitudes of these arrivals to determine the likelihoods of observing them. A particular skip arrival may be predicted but so weakly that it cannot be detected; thus, its inclusion in the travel-time tabulation would add a modeling degree of freedom that does not practically represent the physical system, leading to reduced location residuals but not improved location accuracy.

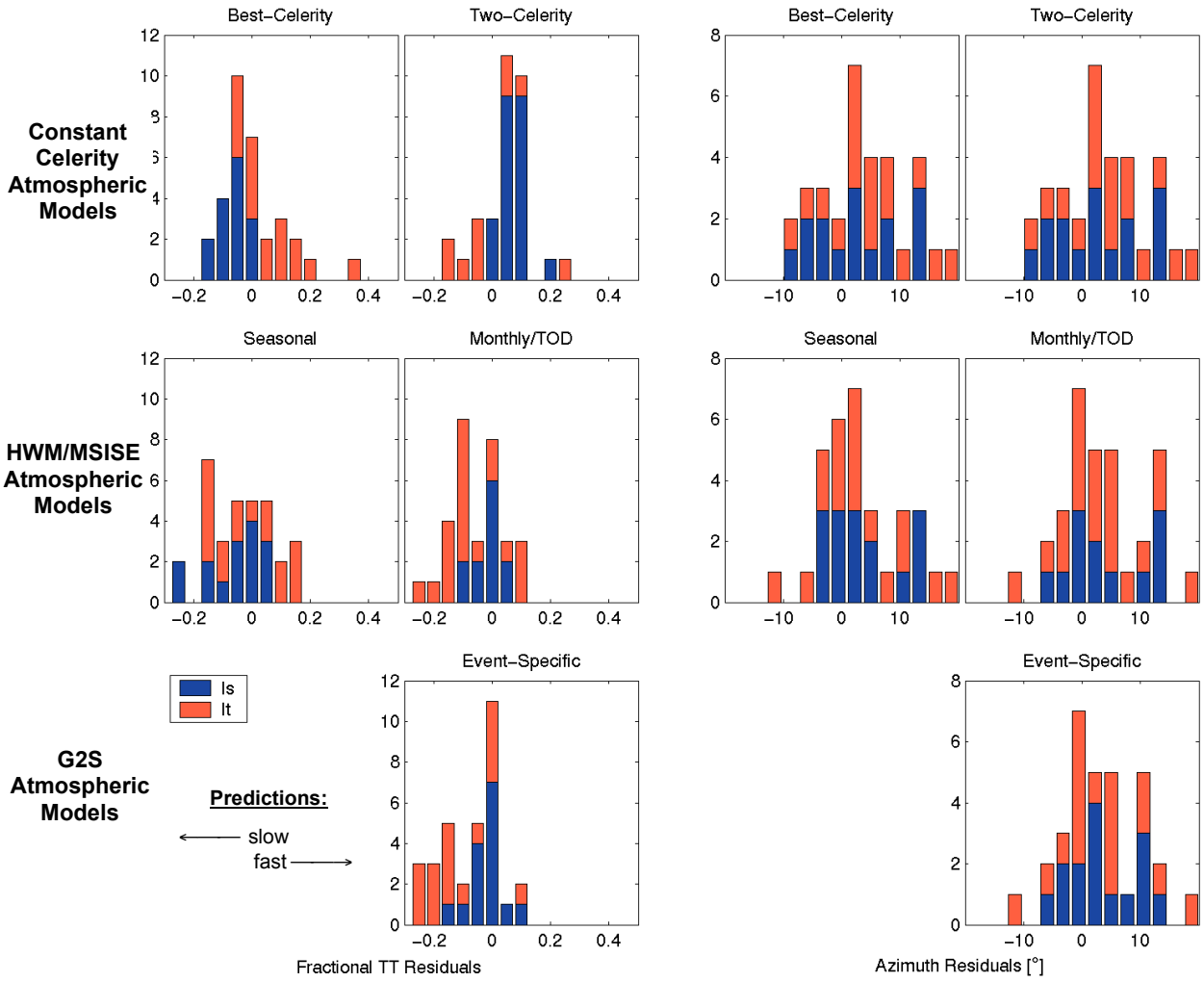

Figure 4. Back azimuth residuals and fractional travel-time residuals.
(a) Fractional travel-time residuals, (ground-truth – observed) / (ground-truth) and (b) back azimuth residuals computed from the propagation models in Table 1. Counterclockwise from the top left, frames in each panel correspond to the following propagation models: the Two-Celerity (245, 320 m/s), the Best-Celerity (282 m/s), the Monthly/TOD, the Event-Specific model, and the Seasonal models. Inferred "Is" and "It" residuals are blue and red, respectively. Predictions that are faster than observed have positive residuals. The distinctly different shapes, spreads and biases of the distributions of "Is" and "It" residuals suggests that significant error may result from averaging multiple skip paths within each propagation duct.

There are other possible sources of the observed residuals. There is some error in the manually determined "ground truth" arrival times and azimuths despite close examination – arrivals from the Thiokol static rocket motor test and the three rocket-launch events have low signal-to-noise, so those picks have lower confidence associated with them. In addition, our ground-truth locations have some uncertainty for events such as the three rocket launches, which are moving sources. Ground-truth errors will be manifest in the residuals from all models but somewhat unpredictably, possibly in a uniform manner introducing an overall residual water level, possibly introducing or even countering model-specific biases. It is also possible that the Tau-P based ray-tracing approach we used make too many approximations to obtain accurate travel times. We have only crudely accounted for along-path velocity variations, and not at all for changes in the direction of the wave front as is possible with other methods.

CONCLUSIONS AND RECOMMENDATIONS

We computed a new set of global infrasound travel-time tables based on a monthly and time-of-day sampling of HWM/MSISE to replace the tables of Brown (2000). The new tables produced more accurate estimates of travel times and back azimuths than the old tables at the 70% confidence level. We compared the predictive capabilities of five atmospheric propagation models of varied complexity on the same set of ground-truth events. The performance of these from best to worst as follows: the new Monthly/TOD model based on HWM/MSISE, the Two-Celerity model of 245 and 320 m/s, the new Event-Specific model based on G2S models, the best fitting constant celerity of 282 m/s, and the Seasonal HWM/MSISE model of Brown (2000). However none is better than any other with confidence of more than 71%. The significance of these results is limited due to the small size of the evaluation data set, particularly with respect to the amount of variability inherent in infrasound propagation. We recommend that more ground truth data be sought and compiled for the purpose of evaluating the predictive abilities of propagation models.

We suspect that a significant amount of the total residual from the new HWM/MSISE and G2S based travel times is the result of approximating of the multiple skip paths within each atmospheric duct by one infrasonic phase, and that this partly obscures the accuracy inherent in the atmospheric velocity models. We recommend investigating location improvement by independently representing travel time and back azimuth corrections for each skip path and studying predicted arrival amplitude to identify the paths with high probability of detection.

We also suspect that approximations in the method we employed for propagating infrasound through a spatially variant atmosphere contributes significantly to the observed residual with respect to ground-truth. We recommend investigation of prediction improvement through the application of more sophisticated propagation methods.

ACKNOWLEDGEMENTS

We thank Doug Drob of the Naval Research Laboratory for generating the G2S atmospheric models used in this work and Milton Garces for comments on an early draft.

REFERENCES

Brown, D.J. (2000), PIDC 7.0 – Station specific, 2-D infrasound travel-time tables, *Center for Monitoring Research*, CCB-PRO-00/19Rev. 1.

Drob, D.P. (2003), Detailed specification of the atmosphere for infrasound propagation modeling, *Proceedings of the 25th Annual Seismic Research Review – Nuclear Explosion Monitoring: Building the Knowledge Base*, LA-UR-03-6029, Vol. II, pp. 605-616.

Garces, M.A., R.A., Hansen, and K.G. Lindquist (1998), Traveltimes for infrasonic waves propagating in a stratified atmosphere, *Geophys. J. Int*., 135, 255-263.

Hedin, A. E, E. L. Fleming, A. H. Manson, F. J. Schmidlin, S. K. Avery, R. R. Clark, S. J. Franke, G. J. Fraser, T. Tsuda, F. Vial, and R. A. Vincent (1996), Empirical wind model for the upper, middle, and lower atmosphere, *J. Atmos. Terr. Phys*., 58, 1421-1447.

Hetzer, C. and M. Garces (2002), Tau 9.1 Users Manual, Infrasound Laboratory, University of Hawaii, Manoa, October 21.

Jones, R. M., J. P. Riley, and T. M. Georges, (1986), HARPA -- A versatile three-dimensional Hamiltonian ray-tracing program for acoustic waves in the atmosphere above irregular terrain*, NOAA Special Report*, 410.

Picone, J.M., A.E. Hedin, D.P. Drob, and A.C. Aikin, (2002) NRLMSISE-00 Empirical model of the atmosphere statistical comparisons and scientific issues, *J. Geophys. Res*., 107, no. 1468, doi:10.1029/2002JA009430.